Possible Superconductivity in Biphenylene

Jiacheng Ye(叶家成)[1], Jun Li(李军)[2*], DingYong Zhong(钟定永)[1], and Dao-Xin Yao(姚道新)[1,3*]

[1]*State Key Laboratory of Optoelectronic Materials and Technologies, Guangdong Provincial Key Laboratory of Magnetoelectric Physics and Devices, School of Physics, Sun Yat-Sen University, Guangzhou 510275, China*
[2]*Key Laboratory for Microstructural Material Physics of Hebei Province, School of Science, Yanshan University, Qinhuangdao 066004, China*
[3]*International Quantum Academy, Shenzhen 518048, China*

(Received 13 April 2023; accepted manuscript online 27 June 2023)

A new two-dimensional allotrope of carbon known as biphenylene has been synthesized. Building on previous research investigating the superconductivity of octagraphene with a square-octagon structure, we conduct a systematic study on possible superconductivity of biphenylene with partial square-octagon structure. First-principle calculations are used to fit the tight-binding model of the material and to estimate its superconductivity. We find that the conventional superconducting transition temperature T_c based on electron-phonon interaction is 3.02 K, while the unconventional T_c primarily caused by spin fluctuation is 1.7 K. We hypothesize that the remaining hexagonal C_6 structure of biphenylene may not be conducive to the formation of perfect Fermi nesting, leading to a lower T_c. The superconducting properties of this material fall between those of graphene and octagraphene, and it lays a foundation for achieving high-temperature superconductivity in carbon-based materials.

DOI: 10.1088/0256-307X/40/7/077401

Carbon is a remarkable element capable of forming numerous structures, including one-dimensional sp, two-dimensional sp^2 hybrid, and three-dimensional sp^3 hybrid bonding. In the field of two-dimensional (2D) materials, carbon-based materials play a significant role, with graphene being the first 2D material reported due to its honeycomb structure resulting from the natural triple rotational symmetry of sp^2 hybrid bonds forming the stable hexagonal C_6 rings. Over the past two decades, a large number of 2D carbon-based materials with triple rotational symmetry hexagonal C_6 rings have been discovered,[1,2] and some of these configurations have been realized experimentally. Additionally, there are numerous 2D materials with other carbon rings that are slightly less stable, including pentagon C_5 and heptagon C_7 ring structures,[3,4] as well as square C_4 and C_8 ring structures.[5,6] Octagraphene, for instance, which is composed of pure square C_4 and C_8 rings, has received extensive attention due to its potential for high Fermi velocity, high-temperature superconductivity, and topology matter.[6–8]

In recent years, carbon-based materials have received considerable attention due to their remarkable properties. Fan *et al.* reported a significant breakthrough in the synthesis of octagraphene-like structures by synthesizing biphenylene, a 2D carbon allotrope with a 4–6–8 structure.[9] Biphenylene is composed of rectangular, hexagonal, and octagonal rings, and its lattice is a rectangular lattice with a lower symmetry of D_{2h} point group, which is different from the regular hexagonal or square lattice. After the synthesis of biphenylene, extensive first-principles and molecular dynamics studies have been conducted on its mechanical, catalytic, electronic, and phonon transport properties. The cohesive energy of monolayer biphenylene is 7.40 eV/atom, and its mechanical properties decrease with increasing temperature due to the increase in interatomic distance and reduction in binding energy.[10] Biphenylene exhibits obvious electronic and phonon transport anisotropy along the armchair and zigzag directions. The phonon thermal conductivity κ_{ph} of biphenylene is lower than that of graphene, which is attributed to its lower lattice symmetry.[11–13] However, its total thermal conductivity κ_{total}, which includes both phonon and electron thermal conductivity, is similar to that of graphene. Biphenylene also demonstrates excellent catalytic properties due to its good metallic properties. For instance, it can be used in hydrogen evolution reaction with atomic doping,[14,15] CO_2 reduction reaction with Fe atoms doping,[16] and electrochemical nitrogen reduction reaction with Mo atoms doping.[17] Furthermore, it can be applied in superlattice nanostructures to achieve lower thermal conductivity for nanodevices.[18,19]

In addition to the fascinating properties mentioned above, the superconducting properties of biphenylene must be explored. To gain a better understanding of its lattice structure, an alternative perspective should be taken. Apart from the hexagonal C_6 rings, biphenylene contains C_4–C_8 ring pairs that can be viewed as an intermediate product between graphene and octagraphene. When the electronic energy bands of graphene are half-filled, it displays a unique Dirac cone electronic band structure, resulting in a lack of density of states near the Fermi surface, which renders graphene unable to exhibit superconductivity. However, when modified through doping[20]

*Corresponding authors. Email: ljcj007@ysu.edu.cn; yaodaox@mail.sysu.edu.cn
© 2023 Chinese Physical Society and IOP Publishing Ltd

or twisting,[21] graphene displays exciting superconductivity due to its strong coupling of sp^2 hybrid bonding, electron–phonon interaction, or on-site Coulomb interaction between $2p_z$ electrons.[22,23] On the other hand, our previous study on octagraphene has revealed that it has perfect Fermi surface nesting, and long-range magnetic order is disrupted through electron doping, which could result in unconventional $s^{\pm}$ superconductivity based on spin fluctuation at high temperatures. Additionally, even conventional superconductivity based on electron-phonon coupling (EPC) can be observed in octagraphene.[7,24,25] Given that biphenylene's lattice structure is intermediate between graphene and octagraphene, it is intriguing to investigate whether biphenylene exhibits high-temperature superconductivity due to EPC or spin and charge fluctuations. Moreover, unlike graphene, biphenylene has a good density of states near the Fermi surface and strong on-site Coulomb interaction in the $2p_z$ orbital. Furthermore, the weak Fermi surface nesting in biphenylene is not conducive to magnetic ordering, which leads to some magnetic fluctuations that may result in unconventional electron pairing and the emergence of superconductivity. Based on these findings, we are confident that superconductivity can be achieved in biphenylene.

In this Letter, we report a systematic investigation of the electronic band structure and superconductivity properties of biphenylene. To accomplish this, we use both density-functional theory (DFT) and tight-binding (TB) models to calculate the electronic band structures of biphenylene. To determine the hopping energies, we employ DFT band structures to fit those of the TB model. In addition, we provide detailed introductions and calculations of the random phase approximation (RPA) approach based on spin or charge fluctuations for pairing. Our results demonstrate that biphenylene possesses good density of states near the Fermi surface and weak Fermi surface nesting similar to doped octagraphene. These characteristics suggest the potential for low-temperature conventional superconductivity induced by EPC, as well as unconventional superconductivity based on spin and charge fluctuations. Our research on biphenylene aims to not only explore its potential as a carbon olefin superconductor but also to verify the reliability of our previous research on various properties of octagraphene, such as investigating whether octagraphene exhibits unconventional superconductivity at higher temperatures, as we have previously predicted. Overall, our findings provide valuable insights into the electronic properties of biphenylene and pave the way for further experimental exploration of its superconductivity properties.

To perform DFT calculations, we use the projector-augmented wave method implemented in the Vienna *ab initio* simulation package (VASP).[26–29] The generalized gradient approximation and the Perdew–Burke–Ernzerhof function are used to treat the electron exchange correlation potential.[30] An extremely high cutoff energy (1500 eV) and $16 \times 14 \times 1$ k-point mesh with the Monkhorst–Pack scheme are used in the self-consistent calculation. The vacuum is set at 15 Å to avoid external interaction. EPC calculations are performed in the framework of density functional perturbation theory (DFPT), as implemented in the *quantum-espresso* code.[31,32]

We start from calculating the lattice parameters and electronic band structures of biphenylene by DFT, as shown in Fig. 1. Biphenylene belongs to 2D rectangular space group pmm or $p6mm$, compared with graphene (2D hexagonal space group $p6m$) or octagraphene (2D square space group $p4m$). As a result, there is no dual degenerate of energy band at Γ or M point. We note that the energy band of biphenylene shows that the K–M line and Γ–K' line intersect the Fermi level. It forms a pair of pockets near K' and M, similar to octagraphene. Unlike octagraphene, the material does not form a perfect Fermi surface nesting, but a weak Fermi surface nesting with vector $(0, \pi)$. The phenomenon of Fermi nesting has been observed in iron-based superconductors, which leads us to believe that the biphenylene material has certain superconducting pairing and transition temperature (T_c).

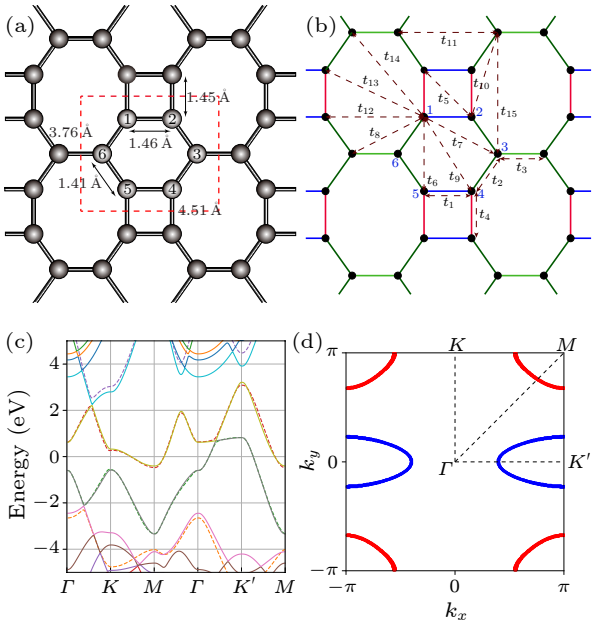

Fig. 1. (a) The lattice structure of biphenylene and the size from DFT calculation. (b) The hopping energies from t_1 to t_{15} for TB model, fitted by DFT calculation. (c) Band structures of biphenylene. DFT calculated results, solid lines; fitting results obtained by TB model, dashed lines. (d) Fermi Surface of biphenylene from TB calculations. The red curves and blue curves represent the electron pocket and the hole pocket, respectively.

We build a TB model to describe biphenylene. As illustrated in Fig. 1(a), we consider a rectangular unit cell of biphenylene represented by the red line, which contains six carbon atoms. The lattice parameters are calculated by DFT. Generally, we construct the TB Hamiltonian for electrons in biphenylene as

$$H_{\mathrm{TB}} = -\sum_{i,j,\sigma} t_{ij} c^{\dagger}_{i\sigma} c_{j\sigma} + \mathrm{H.c.}, \tag{1}$$

where $c^{\dagger}_{i\sigma}$ ($c_{i\sigma}$) represents the creation (annihilation) of an electron with spin σ at site i.

Table 1. Hopping energies and distances for TB model, with x and y representing the hopping distances in units of cell size.

	t_1	t_2	t_3	t_4	t_5	t_6	t_7	t_8	t_9	t_{10}	t_{11}	t_{12}	t_{13}	t_{14}	t_{15}
Energy (eV)	2.273	3.444	4.947	2.990	−0.255	0.623	−0.315	0.578	−0.310	−0.502	0.937	0.236	0.216	0.545	0.128
Distance (Å)	1.455	1.402	1.439	1.449	2.053	2.298	2.534	2.521	2.720	2.720	3.061	3.049	3.434	3.376	3.747
x	0.324	0.178	0.320	0	0.324	0	0.502	0.498	0.324	0.178	0.680	0.676	0.676	0.498	0
y	0	0.307	0	0.386	0.386	0.614	0.307	0.307	0.614	0.693	0	0	0.386	0.693	1

We consider 15 different hopping energies t_{ij} (from t_1 to t_{15}) to achieve a more accurate fit between the curves obtained by DFT and TB calculations. This improves the accuracy of our RPA calculation. In fact, it solves the issue of flat bands appearing near the Fermi surface along the Γ–K' line with fewer TB parameters, where there should be a Dirac cone.[33] The $2p_z$ orbital of carbon contributes the electron states near the Fermi level, so the TB model is of single orbital. By Fourier transform, the TB Hamiltonian of biphenylene reads

$$\widetilde{H}_{\mathrm{TB}} = -\begin{bmatrix} H_{11} & H_{12} & \cdots & H_{16} \\ H_{21} & H_{22} & \cdots & H_{26} \\ \vdots & \vdots & \ddots & \vdots \\ H_{61} & H_{62} & \cdots & H_{66} \end{bmatrix}, \tag{2}$$

where

$$H_{ij} = \sum_{[i,j]} t_{[i,j]} e^{i\boldsymbol{k}\cdot\boldsymbol{a}_{[i,j]}}. \tag{3}$$

The sum of $[i,j]$ here is taken over all hopping parameters associated with the i,j lattice points. For example, $H_{12} = t_1 e^{i\boldsymbol{k}\cdot\boldsymbol{a}_{12}} + t_{12} e^{i\boldsymbol{k}\cdot\boldsymbol{a}'_{12}}$, where $\boldsymbol{a}_{12}$ and $\boldsymbol{a}'_{12}$ represent the vectors from lattice point 1 to 2, corresponding to hopping energies t_1 and t_{12}, respectively. For the TB Hamiltonian $\widetilde{H}_{\mathrm{TB}}$, $H_{ij} = H^*_{ji} (i,\, j = 1,\, 2,\, 3,\, 4,\, 5,\, 6)$ because of its Hermitian property.

The estimated hopping energies for the TB model are given in Table 1, by fitting the band structure using that calculated by DFT. As can be seen, though it is so far for electrons to hop from site to site with the hopping amplitude t_{15}, it does contribute to the energy states.

Six energy bands of biphenylene are obtained by diagonalizing the TB Hamiltonian. We focus on the two bands across the Fermi level, as they contribute to the Fermi surface of biphenylene. It does not has a perfect Fermi surface nesting. The Fermi surface in the first Brillouin zone is formed with an electron pocket and a hole pocket, with the nesting vector $\boldsymbol{Q} \approx (0, \pi)$.

Like graphene and octagraphene, biphenylene also exhibits Coulomb interaction between its $2p_z$ electrons,[34–36] which is of great importance for understanding defect-induced magnetism.[37,38] To account for these effects, we employ a Hubbard model

$$H_{\mathrm{Hubbard}} = H_{\mathrm{TB}} + U \sum_i \hat{n}_{i\uparrow} \hat{n}_{i\downarrow}, \tag{4}$$

where U denotes the on-site repulsive interaction between the $2p_z$ electrons. We approximate the spin and charge susceptibility of the system using RPA, which allows us to obtain the effective pairing interaction of electrons via their fluctuation exchange. At the RPA level, accounting for the on-site repulsive interaction between electrons, the spin susceptibility and charge susceptibility can be obtained through the Dyson equation expressed as follows:

$$\begin{aligned} \chi^{\mathrm{s}}(\boldsymbol{q}) &= \left[I - \chi^0(\boldsymbol{q})\widetilde{U}^{\mathrm{s}}\right]^{-1} \chi^0(\boldsymbol{q}), \\ \chi^{\mathrm{c}}(\boldsymbol{q}) &= \left[I + \chi^0(\boldsymbol{q})\widetilde{U}^{\mathrm{c}}\right]^{-1} \chi^0(\boldsymbol{q}). \end{aligned} \tag{5}$$

Here, $\chi^{\mathrm{s}}(\boldsymbol{q})$, $\chi^{\mathrm{c}}(\boldsymbol{q})$, $\chi^0(\boldsymbol{q})$, $\widetilde{U}^{\mathrm{s}}$, and $\widetilde{U}^{\mathrm{c}}$ are 36×36 matrices, with $\widetilde{U}^{(\mathrm{s})l_1 l_2}_{l_3 l_4} = \widetilde{U}^{(\mathrm{c})l_1 l_2}_{l_3 l_4} = \widetilde{U}^{l_1 l_2}_{l_3 l_4} = U\delta_{l_1=l_2=l_3=l_4}$ in our model; l_1–l_4 are the orbital indexes, and each of them refers to the 6 lattice points in the unit cell; $\chi^0(\boldsymbol{q})$ is the free susceptibility for $U = 0$, which can be defined as

$$\chi^{(0)l_1 l_2}_{l_3 l_4}(\boldsymbol{q}) = \frac{1}{N} \sum_{\boldsymbol{k},\alpha,\beta} \xi^{\alpha}_{l_4}(\boldsymbol{k}) \xi^{\alpha,*}_{l_3}(\boldsymbol{k}) \xi^{\beta}_{l_2}(\boldsymbol{k}') \xi^{\beta,*}_{l_1}(\boldsymbol{k}') \times \frac{n_{\mathrm{F}}(\varepsilon^{\beta}_{\boldsymbol{k}'}) - n_{\mathrm{F}}(\varepsilon^{\alpha}_{\boldsymbol{k}})}{\varepsilon^{\alpha}_{\boldsymbol{k}} - \varepsilon^{\beta}_{\boldsymbol{k}'}}, \tag{6}$$

where α and β refer to the six TB bands of biphenylene; $\xi^{\alpha}(\boldsymbol{k})$ and $\varepsilon^{\alpha}_{\boldsymbol{k}}$ denote the αth eigenvector and eigenvalue obtained from the TB Hamiltonian, respectively; and $\boldsymbol{k}' = \boldsymbol{k} + \boldsymbol{q}$. The Fermi distribution function is denoted by n_{F}.

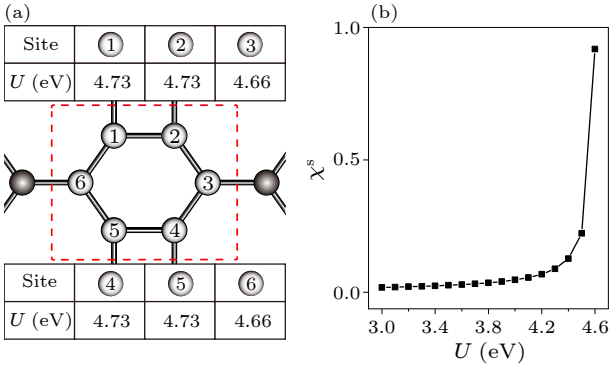

Fig. 2. (a) The effective Coulomb interactions U at different sites, obtained by cRPA calculations. (b) The variation of the maximum eigenvalue of the spin susceptibility χ^{s} with respect to the interaction U, where the ordinate represents the relative values of the spin susceptibility.

It should be noted that RPA is only applicable to a weak-coupling system. For the spin susceptibility in Eq. (5), a critical interaction U_{c} can be determined. When $U > U_{\mathrm{c}}$, the spin susceptibility diverges. We obtain $U_{\mathrm{c}} = 4.67\,\mathrm{eV}$ with half-filling in our calculations and we set $U = 4.0\,\mathrm{eV}$. The actual value of U in biphenylene is more likely to be larger.[34,39–41] We utilize the constrained random phase approximation (cRPA) to evaluate the interaction parameter U,[42] as illustrated in Fig. 2(a). However, due to the weak-coupling character of RPA, the spin susceptibility tends to diverge and be overestimated when U approaches U_{c} [Fig. 2(b)], resulting in excessive spin fluctuation. This often leads to an overestimation of T_{c}. Therefore, it is more appropriate to obtain T_{c} using a smaller U

value of 4.0 eV, ensuring that the spin fluctuation is neither too high nor too low. In fact, in our previous calculation for the single layer octagraphene, we obtain the similar results with the gap $\Delta \approx 50$ meV based on weak-coupling RPA for $U = 4.5$ eV and variational Monte Carlo method for $U = 10$ eV.[7]

We define the static susceptibility matrix as

$$\chi^0_{lm}(\boldsymbol{q}) \equiv \chi^{(0)l,l}_{m,m}(\boldsymbol{q}), \tag{7}$$

and its largest eigenvalue $\chi(\boldsymbol{q})$ represents the eigensusceptibility in the strongest channel. We can find that in the first Brillouin zone shown in Fig. 3(a), the peak of $\chi(\boldsymbol{q})$ lies in $(0,\pi)$, corresponding to the $(0,\pi)$ nesting vector.

Spin or charge fluctuation causes a Cooper pair to scatter from $\boldsymbol{k}'$, orbital (t,s) to $\boldsymbol{k}$, (p,q). The Cooper pair can be a spin singlet or a spin triplet. At the RPA level, the effective interaction can be expressed as

$$V_{\text{eff}} = \frac{1}{N}\sum_{pqst,\boldsymbol{k}\boldsymbol{k}'} \Gamma^{pq}_{st}(\boldsymbol{k},\boldsymbol{k}')c^\dagger_p(\boldsymbol{k})c^\dagger_q(-\boldsymbol{k})c_s(-\boldsymbol{k}')c_t(\boldsymbol{k}'), \tag{8}$$

where the effective vertex $\Gamma^{pq}_{st}(\boldsymbol{k},\boldsymbol{k}')$ can be obtained by RPA susceptibility. In the singlet channel, it is given as follows:

$$\begin{aligned}\Gamma^{pq}_{st}(k,k') = {}& \widetilde{U}^{pt}_{qs} + \frac{1}{4}\{\widetilde{U}[3\chi^{\text{s}}(k-k') - \chi^{\text{c}}(k-k')]\widetilde{U}\}^{pt}_{qs} \\ & + \frac{1}{4}\{\widetilde{U}[3\chi^{\text{s}}(k+k') - \chi^{\text{c}}(k+k')]\widetilde{U}\}^{ps}_{qt}. \end{aligned} \tag{9}$$

In the triplet channel,

$$\begin{aligned}\Gamma^{pq}_{st}(k,k') = {}& -\frac{1}{4}\{\widetilde{U}[\chi^{\text{s}}(k-k') + \chi^{\text{c}}(k-k')]\widetilde{U}\}^{pt}_{qs} \\ & + \frac{1}{4}\{\widetilde{U}[\chi^{\text{s}}(k+k') + \chi^{\text{c}}(k+k')]\widetilde{U}\}^{ps}_{qt}. \end{aligned} \tag{10}$$

In the energy representation, we obtain the projection of the effective vertex $\Gamma^{pq}_{st}(\boldsymbol{k},\boldsymbol{k}')$ in the energy eigenstate

$$\begin{aligned}V^{\alpha\beta}(\boldsymbol{k},\boldsymbol{k}') = \text{Re}\sum_{pqst,\boldsymbol{k}\boldsymbol{k}'} & \Gamma^{pq}_{st}(\boldsymbol{k},\boldsymbol{k}',0)\xi^{\alpha,*}_p(\boldsymbol{k})\xi^{\alpha,*}_q(-\boldsymbol{k}) \\ & \cdot \xi^{\beta}_s(-\boldsymbol{k}')\xi^{\beta}_t(\boldsymbol{k}'), \end{aligned} \tag{11}$$

where $\alpha,\beta = 1,2$ indicate the states in the two bands which cross the Fermi surface (FS). The gap function is constructed as

$$-\frac{1}{(2\pi)^2}\sum_\beta \oint_{\text{FS}} dk'_\parallel \frac{V^{\alpha\beta}(\boldsymbol{k},\boldsymbol{k}')}{v^\beta_{\text{F}}(\boldsymbol{k}')}\Delta_\beta(\boldsymbol{k}') = \lambda\Delta_\alpha(\boldsymbol{k}), \tag{12}$$

where $k'_\parallel$ indicates that the integration is along the Fermi surface, and v^β_{F} is the Fermi velocity. For each $\boldsymbol{k}$ on the Fermi surface, there is a corresponding gap equation. Thus, Eq. (12) is an eigenequation. The eigenvector $\Delta(\boldsymbol{k})$ represents the relative value of the gap function, which determines the pairing symmetry. The eigenvalue λ represents the width of the gap, while the largest λ has the following correlation with the superconducting T_{c}:

$$\lambda^{-1} = \ln\left(1.13\frac{\hbar\omega_{\text{D}}}{k_{\text{B}}T_{\text{c}}}\right). \tag{13}$$

We set $\hbar\omega_{\text{D}} = 0.3$ eV, as it is the typical energy scale of spin fluctuation.[43] The D_2 point group has 4 irreducible representations, i.e., A_1 corresponding to s-wave pairing, and A_2, B_1, B_2 corresponding to p-wave pairing.[44] In our biphenylene calculation, the largest λ value for s-wave pairing is found to be 0.13, while the largest value for p-wave pairing is 0.11, using Eq. (12). The singlet channel is dominant, and the leading pairing symmetry is shown as the s-wave [Fig. 3(c)]. From Eq. (13), we obtain $T_{\text{c}} \simeq 1.7$ K, and $\Delta \simeq 0.26$ meV.

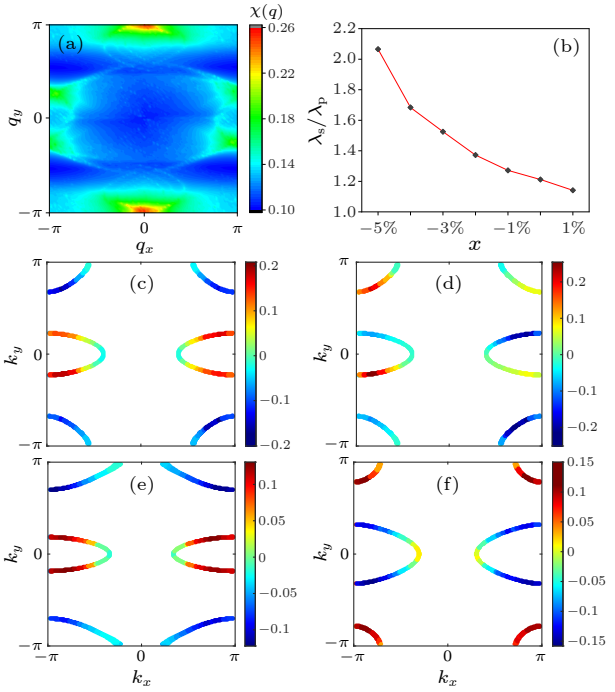

Fig. 3. (a) The $\boldsymbol{q}$-dependence of the largest eigensusceptibility $\chi(\boldsymbol{q})$ [see Eq. (7)] in the first Brillouin zone. (b) The ratio of the largest λ for s-wave pairing to that of p-wave pairing. [(c), (d)] The gap function $\Delta(\boldsymbol{k})$ projected on the Fermi surface for $\lambda = 0.13$ and 0.11 corresponding to s-wave pairing and p-wave pairing, respectively. [(e), (f)] The gap function $\Delta(\boldsymbol{k})$ with doping $x = +0.01$, $x = -0.05$, respectively.

Electron or hole doping is a widely used approach in investigating unconventional superconductivity. We conduct calculations to investigate the unconventional superconducting properties of biphenylene with a low level of doping, since excessive electron doping can destroy the Fermi pockets. Our results reveal that within a certain range, hole doping favors s-wave pairing, whereas electron doping promotes p-wave pairing, as depicted in Fig. 3(b). The ratio of the largest λ for s-wave pairing to that of p-wave pairing, $\lambda_{\text{s}}/\lambda_{\text{p}}$, increases with hole doping and decreases with electron doping.

We have thoroughly investigated the superconducting properties of the material and found that it exhibits relatively low unconventional superconductivity under a wide range of conditions. These findings are in contrast to our previous studies on octagraphene with a square-octagon structure, which exhibits much higher levels of unconventional superconductivity.[7,24,25] From a symmetry perspective, the material possesses lower symmetry compared to both graphene and octagraphene, making it less favorable for the formation of an ideal (π,π) Fermi surface nest-

ing. Therefore, only a rough Fermi surface nesting can be formed in a single direction. In semi-metallic graphene, only one Fermi pocket appears due to its hexagonal honeycomb arrangement and strong doping, which makes it difficult for Fermi surface nesting to occur. On the other hand, thanks to the high symmetry and square-octagon structure, octagraphene exhibits perfect intrinsic Fermi surface nesting. Even if the C_4–C_8 ring is stretched in biphenylene, it does not disrupt the Fermi surface nesting. However, the presence of six-membered rings in biphenylene reduces its symmetry in comparison to octagraphene, leading to inadequate nesting of Fermi surface.

For comparison, we investigate its conventional superconducting properties by EPC calculations and the Allen–Dynes modified McMillan equation. By integrating the Eliashberg function $\lambda = 2\int \frac{\alpha^2F(\omega)}{\omega}d\omega$, we get the EPC strength $\lambda = 0.81$. According to the BCS theory, the Allen–Dynes T_c is estimated to be 3.02 K by the McMillan equation [45]

$$T_c = \frac{\omega_{\log}}{1.2}\exp\Big[-\frac{1.04(1+\lambda)}{\lambda-\mu^*(1+0.62\lambda)}\Big]. \tag{14}$$

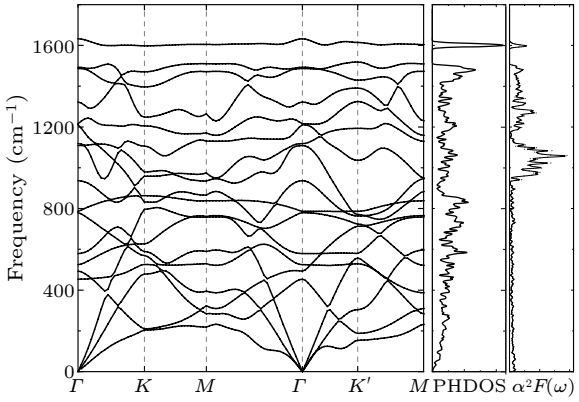

Fig. 4. The phonon spectrum of biphenylene, phonon density of states (PHDOS) and Eliashberg spectral function $\alpha^2F(\omega)$.

In stark contrast to biphenylene, octagraphene has a larger EPC constant (λ) of 1.23 and a higher superconducting T_c of 20.8 K. [46] Our findings suggest that the electron–phonon superconductivity of biphenylene mainly originates from the medium frequency range, which differs from octagraphene, where the low frequency range dominates. This discrepancy can be attributed to the absence of a pure six-membered ring structure in the square-octagon structure of octagraphene. Additionally, the C–C bond energy in graphene is higher than that in the loose C–C bond of the square-octagon structure, resulting in differences in the EPC calculations. Although biphenylene exhibits some degree of electron–phonon superconductivity, it is significantly lower than that of standard octagraphene with a square-octagon structure.

To sum up, motivated by previous research on superconductivity in octagraphene with a square-octagon structure, we have systematically investigated the potential superconductivity of biphenylene with a partial square-octagon structure. We employ first-principles calculations to fit the TB model of the material and estimate its superconductivity based on EPC and RPA calculations. The conventional superconducting T_c based on EPC is estimated to be 3.02 K, and the unconventional superconducting T_c based on s-wave pairing is estimated to be 1.7 K. We attribute the presence of superconductivity in this material to the Fermi nesting resulting from the square-octagon structure, which is absent in graphene. However, the remaining hexagonal structure is not conducive to the formation of perfect Fermi nesting, leading to a low T_c. Because biphenylene incorporates six-membered rings, its symmetry is reduced compared to that of octagraphene, and hence, it does not display the same level of robust superconductivity as observed in octagraphene. Nevertheless, as a recently synthesized 2D carbon-based material, the discovery of its superconductivity provides a basis for achieving high-temperature superconductivity in similar two-dimensional carbon-based materials.

Acknowledgments. We gratefully thank F. Yang for helpful discussion. This work was supported by the National Key R&D Program of China (Grant Nos. 2018YFA0306001 and 2022YFA1402802), the National Natural Science Foundation of China (Grant Nos. 92165204, 11974431, and 11974432), the Natural Science Foundation of Hebei Province (Grant No. A2021203010), Shenzhen International Quantum Academy (Grant No. SIQA202102), and the Leading Talent Program of Guangdong Special Projects (Grant No. 201626003).

References

[1] Narita N, Nagai S, Suzuki S, and Nakao K 1998 *Phys. Rev. B* **58** 11009
[2] Enyashin A N and Ivanovskii A L 2011 *Phys. Status Solidi B* **248** 1879
[3] Crespi V H, Benedict L X, Cohen M L, and Louie S G 1996 *Phys. Rev. B* **53** R13303
[4] Deza M, Fowler P W, Shtogrin M, and Vietze K 2000 *J. Chem. Inf. Comput. Sci.* **40** 1325
[5] Bucknum M J and Castro E A 2008 *Solid State Sci.* **10** 1245
[6] Liu Y, Wang G, Huang Q, Guo L, and Chen X 2012 *Phys. Rev. Lett.* **108** 225505
[7] Kang Y T, Lu C, Yang F, and Yao D X 2019 *Phys. Rev. B* **99** 184506
[8] de Crasto L F, Ferreira G J, and Miwa R H 2019 *Phys. Chem. Chem. Phys.* **21** 22344
[9] Fan Q T, Yan L H, Tripp M W, Krejci O, Dimosthenous S, Kachel S R, Chen M, Foster A S, Koert U, Liljeroth P, and Gottfried J M 2021 *Science* **372** 852
[10] Hamed M A, Zarghami D M, Molaie F, Fooladapanjeh S, Farzadian O, and Spitas C 2022 *Comput. Mater. Sci.* **214** 111761
[11] Liu G, Chen T, Li X, Xu Z, and Xiao X 2022 *Appl. Surf. Sci.* **599** 153993
[12] Tong Z, Pecchia A, Yam C, Dumitrica T, and Frauenheim T 2022 *Adv. Energy Mater.* **12** 2200657
[13] Veeravenkata H P and Jain A 2021 *Carbon* **183** 893
[14] Luo Y, Ren C, Xu Y, Yu J, Wang S, and Sun M 2021 *Sci. Rep.* **11** 19008
[15] Ren K, Shu H, Huo W, Cui Z, and Xu Y 2022 *Nanotechnology* **33** 345701
[16] Xing N, Liu Z, Wang Z, Gao Y, Li Q, and Wang H 2022 *Phys. Chem. Chem. Phys.* **24** 27474
[17] Feng Z, Ma T, Li R, Zhu M, Shi D, Tang Y, and Dai X 2022 *Mol. Catal.* **530** 112579

[18] Farzadian O, Dehaghani M Z, Kostas K V, Mashhadzadeh A H, and Spitas C 2022 *Nanotechnology* **33** 355705
[19] Zarghami D M, Farzadian O, Kostas K V, Molaei F, Spitas C, and Hamed M A 2022 *Physica E* **144** 115411
[20] Black-Schaffer A M and Honerkamp C 2014 *J. Phys.: Condens. Matter* **26** 423201
[21] Cao Y, Fatemi V, Fang S, Watanabe K, Taniguchi T, Kaxiras E, and Jarillo-Herrero P 2018 *Nature* **556** 43
[22] Ma T X, Yang F, Huang Z B, and Lin H Q 2017 *Sci. Rep.* **7** 19
[23] Yankowitz M, Chen S, Polshyn H, Zhang Y, Watanabe K, Taniguchi T, Graf D, Young A F, and Dean C R 2019 *Science* **363** 1059
[24] Li J, Jin S, Yang F, and Yao D X 2020 *Phys. Rev. B* **102** 174509
[25] Li J and Yao D X 2022 *Chin. Phys. B* **31** 017403
[26] Kresse G and Hafner J 1993 *Phys. Rev. B* **47** 558
[27] Kresse G and Joubert D 1999 *Phys. Rev. B* **59** 1758
[28] Kresse G and Hafner J 1994 *Phys. Rev. B* **49** 14251
[29] Blöchl P E 1994 *Phys. Rev. B* **50** 17953
[30] Perdew J P, Burke K, and Ernzerhof M 1996 *Phys. Rev. Lett.* **77** 3865
[31] Giannozzi P, Baroni S, and Bonini N 2009 *J. Phys.: Condens. Matter* **21** 395502
[32] Piscanec S, Lazzeri M, Mauri F, Ferrari A C, and Robertson J 2004 *Phys. Rev. Lett.* **93** 185503
[33] Liu P F, Li J, Zhang C, Tu X H, Zhang J, Zhang P, Wang B T, and Singh D J 2021 *Phys. Rev. B* **104** 235422
[34] Parr R G, Craig D P, and Ross I G 1950 *J. Chem. Phys.* **18** 1561
[35] Castro N A H, Guinea F, Peres N M R, Novoselov K S, and Geim A K 2009 *Rev. Mod. Phys.* **81** 109
[36] Schüler M, Rösner M, Wehling T O, Lichtenstein A I, and Katsnelson M I 2013 *Phys. Rev. Lett.* **111** 036601
[37] Shibayama Y, Sato H, Enoki T, and Endo M 2000 *Phys. Rev. Lett.* **84** 1744
[38] López-Sancho M P, de Juan F, and Vozmediano M A H 2009 *Phys. Rev. B* **79** 075413
[39] Wehling T O, Şaşıoğlu E, Friedrich C, Lichtenstein A I, Katsnelson M I, and Blügel S 2011 *Phys. Rev. Lett.* **106** 236805
[40] Vardeny Z and Tauc J 1985 *Phys. Rev. Lett.* **54** 1844
[41] Baeriswyl D, Campbell D K, and Mazumdar S 1986 *Phys. Rev. Lett.* **56** 1509
[42] Şaşıoğlu E, Friedrich C, and Blügel S 2011 *Phys. Rev. B* **83** 121101
[43] Liu F, Liu C C, Wu K, Yang F, and Yao Y 2013 *Phys. Rev. Lett.* **111** 066804
[44] Liu Y B, Zhang Y, Chen W Q, and Yang F 2023 *Phys. Rev. B* **107** 014501
[45] Allen P B and Dynes R C 1975 *Phys. Rev. B* **12** 905
[46] Gu Q Y, Xing D Y, and Sun J 2019 *Chin. Phys. Lett.* **36** 097401